Chinese Chemical Letters 34 (2023) 107952

Contents lists available at ScienceDirect

Chinese Chemical Letters

journal homepage: www.elsevier.com/locate/cclet

Colorful ultralong room-temperature phosphorescence in dual-ligand metal-organic framework

Shuya Liu[1], Yuhang Lin[1], Dongpeng Yan*

Beijing Key Laboratory of Energy Conversion and Storage Materials, College of Chemistry, Key Laboratory of Radiopharmaceuticals, Ministry of Education, Beijing Normal University, Beijing 100875, China

ARTICLE INFO

Article history:
Received 7 July 2022
Revised 18 October 2022
Accepted 23 October 2022
Available online 27 October 2022

Keywords:
Room temperature phosphorescence
Information encryption
Metal-organic framework
Up-conversion luminescence
Organic-inorganic hybrids

ABSTRACT

Long afterglow organic-inorganic hybrid materials have attracted much attention in recent years and are widely used in information security, biological imaging and many other fields. Since up-conversion long-persistence materials are promising for bio-optical imaging due to their high penetration depth and elimination of autofluorescence background, it is highly desirable to combine down-conversion and up-conversion pathways to obtain smart materials with excitation-dependent tunable room-temperature phosphorescence properties. In this work, a metal-organic framework (Zn-DCPS-BIMB), consisting of divalent zinc ions, *o*-bis(imidazol-1-ylmethyl)benzene and 4,4′-dicarboxydiphenylsulfone, is designed to stabilize triplet excitons, coordinate the emission of different ligands, and endow materials with tunable emission color and up-conversion properties *via* heavy atoms effects promoting single-triplet orbital coupling and intersystem crossing.

Molecular phosphorescent materials have received a great deal of attention in recent years and are expected to be widely used in information security [1–19], detection [20,21], biology [22–24], and optical devices [25–28]. For example, taking the advantages of ultralong excited-state lifetimes and adjustable afterglow emission colors, molecular phosphors exhibit high-performance in optoelectronic applications such as highly integrated data encryption and multiplexed bioassay [29–33]. To achieve colorful ultralong room-temperature phosphorescence (RTP), most systems have been designed by constructing multiple emission centers [34–36], introduction of external force [37,38], change of temperature [39], and so on. Furthermore, the use of both down-conversion and up-conversion routes to obtain excitation-dependent tunable RTP properties is also highly desirable, since the up-conversion long-afterglow materials are widely used in optical imaging due to the high penetration depth, and elimination of auto-fluorescence background [40,41]. However, the design of multifunctional materials with both tunable long afterglow and excitation-dependent up-conversion luminescence remains a challenging task, and examples are still scare.

Typically, the molecular solid-state luminescence is sensitive to the stacking modes, and the excited state energy can be consumed by intermolecular $\pi-\pi$ interactions or the formation of excimers or exciplexes by other non-radiative channels [42]. In this sense, metal-organic frameworks (MOFs) [43,44] formed by coordination interactions between organic ligands and metals, exhibit highly variable solid-state stacking structures. The metal units in the structure could separate the organic ligands from each other, which increases the rigidity of the structure and reduces the luminescence quenching caused by the aggregation of organic molecules [45–47]. Moreover, the introduction of different photoactive ligands and metal centers could adjust the energy levels and form multiple emission sites, which are beneficial to the color adjustment.

In this work, we have designed dual-ligand MOF Zn-DCPS-BIMB (namely BNU-1) as a new type of long-afterglow material with tunable emission color and up-conversion properties. The MOF with rich luminescent sites consists of divalent zinc ions, *o*-bis(imidazol-1-ylmethyl)benzene (BIMB), and 4,4′-dicarboxydiphenylsulfone (DCPS) (Fig. S1 in Supporting information). The structure contains numbers of carbonyl and heteroatom units, and also has the heavy atom effect from the Zn^{2+} ion. These properties promote the coupling of single-triplet orbitals and facilitate intersystem crossing, thereby stabilizing triplet excitons and obtaining ultralong phosphorescence emission at room temperature. Multiple adjacent energy levels are favorable to energy transfer and conditions for up-conversion luminescence under low-power excitation [48]. The photoluminescence quantum yield (QY_{PL}) and phosphorescence quantum yield (QY_{Phos}) are 2.27% and

* Corresponding author.
E-mail address: yandp@bnu.edu.cn (D. Yan).
[1] These authors contributed equally to this work.

https://doi.org/10.1016/j.cclet.2022.107952
1001-8417/

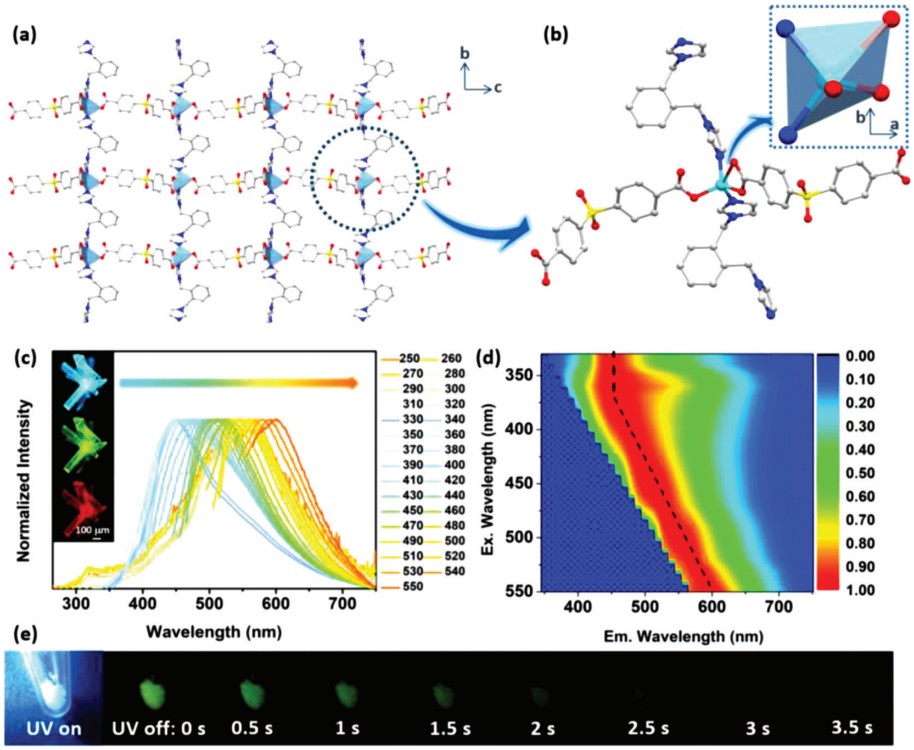

Fig. 1. Structure of Zn-DCPS-BIMB: (a) View of the coordination along *a* axis and (b) the five-coordinated structure. (c) The normalized intensity PL spectra of Zn-DCPS-BIMB under prompt mode at room temperature (λ_{ex} = 250–550 nm). The insert picture is fluorescence microscope pictures under different excitations. (d) The 2D emission contour spectra under prompt mode (intensity is normalized). (e) Photographs taken before and after turning off the UV lamp (λ_{ex} = 254 nm).

1.32% for Zn-DCPS-BIMB, respectively (Table S1 in Supporting information). Both BIMB and DCPS are symmetric organic ligands, but BIMB has a large twisting space for the conformation due to its flexible methylene unit. The single-crystal X-ray diffraction (SCXRD, Table S2 in Supporting information) reveals that, Zn-DCPS-BIMB belongs to orthorhombic system, D_2 point group, $P2_12_12_1$ chiral space group. In each asymmetric unit, Zn^{2+} is five-coordinated (Fig. 1), and appears in a 1:1:1 ratio with BIMB and DCPS. Viewed from the a-axis direction, the coordination polymeric layers are interspersed with each other to form a three-dimensional network structure (Fig. S1). From the b-axis perspective, the DCPS molecules and metal ions form a cellular-like porous unit (Fig. S1c), while the coordinated BIMBs interleave in the pores. The bond lengths and angles in the structure are given in Table S3 (Supporting information). To understand the fixation of flexible organic ligands in rigid structures, we select a part of angles and dihedral angles formed by organic ligands for comparison. The space dihedral angle ∠1 formed by plane 1 composed of Zn-S-Zn and plane 2 composed of Zn-Ph-Zn is 86.859°, indicates possible ligand-to-ligand interactions in the structure. The angles formed by the plane 3 of the benzene ring and the planes 4 and 5 of the two imidazole rings in BIMB are slightly different, which are ∠2 of 78.196° and ∠3 of 77.021°, respectively. Compared with the pristine BIMB, the flexibility of DCPS is reduced, and the two benzene rings and the S atom form the angle. The included angle ∠4 is 104.510°, and the dihedral angle formed by planes 6 and 7 is 71.119° (Fig. S2 in Supporting information). PXRD patterns further verify the successful synthesis of the material (Fig. S3a in Supporting information).

To detect photophysical properties of Zn-DCPS-BIMB, UV-vis absorption spectroscopy was performed (Fig. S3b in Supporting information). Compared with the pristine DCPS and zinc nitrate, its light absorption is greatly extended in the UV-visible range. Unlike the broadening of the absorption range caused by the possible intermolecular interactions of BIMB in pure organics, the organic ligand molecules are separated from each other in the MOF, which result in different absorption intensity compared with raw materials. To verify the MOF-based RTP with color-tunable emission in a wide range, excitation-dependent PL spectra (Fig. 1 and Fig. S4 in Supporting information) and delayed PL spectra (Fig. 2) of the material were tested.

The Zn-DCPS-BIMB presents highly tunable emission color gradually changing from blue to orange as the increase of excitation wavelength (Fig. 1), indicating dual ligands induced orbital coupling and multiple excited states (Figs. S5-S9 in Supporting information). Excitation-dependent luminescence changes also appear in the delayed PL spectrum, where the luminescence color transitions from green to yellow (λ_{ex} = 250-550 nm) (Fig. S10 in Supporting information). As shown in Fig. 2a, green (254 nm excitation) and yellow (365 nm excitation) afterglow emissions further verify the existence of different emission levels in the MOF. Under the excitation at 365 nm, the peak of luminescence spectra appears at 446 nm, while the emission peak of delayed PL spectrum is located at 560 nm (τ = 451.6 ms), corresponding to the yellow position on the CIE color diagram (Fig. S11 in Supporting information). Excitation-dependent decay spectroscopy shows that the maximum emission intensity corresponds to the excitation at 310 nm (Fig. 2a). To investigate the temperature-dependent luminescence at different positions, we tested the temperature-changed decay spectra excited at 310 nm (Table S4, Supporting information). Under ambient conditions, the luminescence spectrum (Fig. 2b) exhibits broad emission peaks at 446, 490 and 535 nm, and the corresponding luminescence color is indicated in Fig. 2c, which further confirms the wide-range luminescent characteristic. The delayed spectrum mainly appears at 490 (τ = 224.3 ms), 535 (τ = 238.2 ms), and 560 nm (τ = 234.8 ms) (Fig. 2d). The emission at 446 nm can be assigned to the delayed fluorescence (DF) emission with both a long lifetime of 59.7 μs (Fig. 2e) and a short lifetime of 6.7 ns (Fig. S12 in Supporting information). Time-

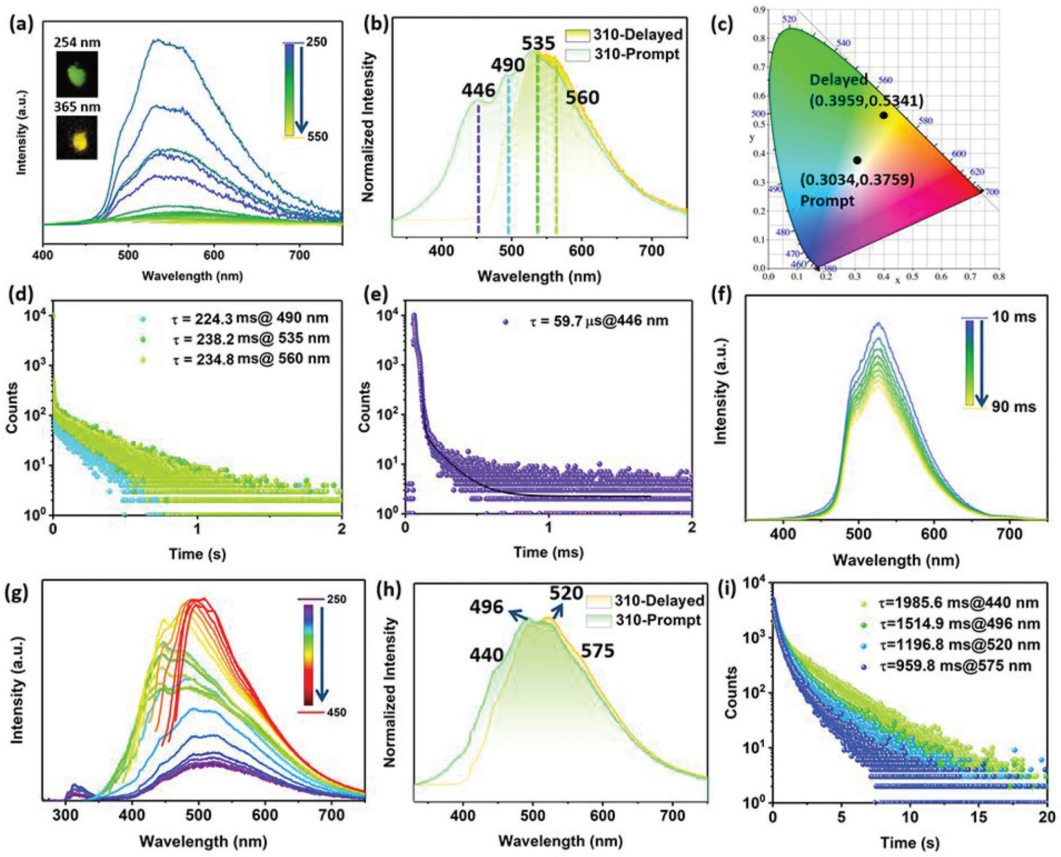

Fig. 2. Zn-DCPS-BIMB: (a) The PL spectra under delayed mode (λ_{ex} = 250-550 nm), the insert pictures are taken after turning off the UV light (λ_{ex} = 254 nm and 365 nm); (b) Prompt and delayed PL spectra excited at 310 nm at ambient condition and (c) the corresponding positions in the chromaticity coordinates diagram (λ_{ex} = 310 nm); (d) The lifetime decay profiles at 485 nm, 535 nm, 560 nm and (e) 446 nm (λ_{ex} = 310 nm); (f) RTP emission spectra at different delayed time (from 10 ms to 90 ms) (λ_{ex} = 310 nm); (g) The PL spectra at 100 K (λ_{ex} = 250-450 nm); (h) Prompt and delayed PL spectra excited at 310 nm at 100 K; (i) The lifetime decay profiles at 440 nm, 496 nm, 520 nm and 575 nm at 100 K (λ_{ex} = 310 nm).

dependent delayed spectra (Fig. 2f) show long-lived luminescence positions stabilized at *ca*. 490, 535 and 560 nm. At a low temperature of 100 K, the thermal vibration in the structure is strongly suppressed, and thus the luminescence spectra (Fig. 2g) show finer structures than that at room temperature (Fig. S4). Under the excitation of 310 nm, the luminescence peaks are stable at 440, 496, 520 and 575 nm (Fig. 2h and Fig. S13 in Supporting information), and the lifetimes are significantly improved compared with those at room temperature, especially that at *ca*. 440 nm increases from 59.7 μs to nearly 2 s (Fig. 2i). Based on the observed spectra, we speculate that 446 nm (S_1) is singlet DF emission [49,50], and 490 (T_3), 535 (T_2) and 560 nm (T_1) are triplet RTP emission (Fig. 3).

There is potential energy transfer path formed by weak $\pi-\pi$ interactions (Fig. S14 in Supporting information) between coordination networks. Particularly, the overlap of excitation-emission spectra (Fig. S15 in Supporting information) between DCPS and BIMB allows occurrence of fluorescence resonance energy transfer (FRET). These enable chromophores a wide range of photoactive sites participating in the process of radiative transitions, consistent with the excitation-dependent luminescence properties. To further verify the above statement, we performed density functional theory (DFT) calculations on Zn-DCPS-BIMB. As shown in Fig. 3a, the electronic state distributions of the same coordination unit in different networks are not identical and relatively dispersed, further demonstrating the extensive energy transfer process between organic ligands. The highest occupied molecular orbitals (HOMOs) are mainly located on the BIMB, while the lowest unoccupied molecular orbitals (LUMOs) are mainly located on the DCPS, which is consistent with the broad UV-vis absorption spectrum (Fig. S3 in Supporting information) and PL spectrum (Figs. 1 and 2) in experiment, revealing the sources of excitation-dependent long-lived RTP in Zn-DCPS-BIMB.

Photons of higher energy than the excitation photons are emitted during the anti-Stokes PL (or photon up-conversion). UV-vis absorption spectra (Fig. S3) and excitation-dependent emission spectra (Figs. 1 and 2) indicate that Zn-DCPS-BIMB has broad absorption in the visible region and complex coupled orbitals, possibly generating short-wave up-conversion emission through long-wave excitation. Here, long-wavelength excitation of Zn-DCPS-BIMB using a 650 nm laser with progressively increasing excitation power yields an up-conversion PL as shown in Fig. 3b. Taking luminescence at the 496 nm as an example, the log (intensity) *versus* log (excitation incident energy) data were fitted as a linear relationship, with slopes of 0.713, indicating that the radiative transition from the excited state to the ground state involves a phonon-assisted single-photon process [51–53]. Phonon-assisted up-conversion luminescence is a process in which the material absorbs low-energy photons while storing the heat in the excitation light in the form of lattice vibrations, thereby enhancing the possibility of single-photon up-conversion (Fig. 3c) [53].

Based on the excitation-dependent ultralong RTP of Zn-DCPS-BIMB, and the difference in the color of the long afterglow emission between different MOF materials, we have designed a multifunctional encryption pattern for information storage. "Sun" in ancient Chinese oracle bone inscriptions is represented by a dot in a circle, the outer circle is like the edge of the sun, and the dot in

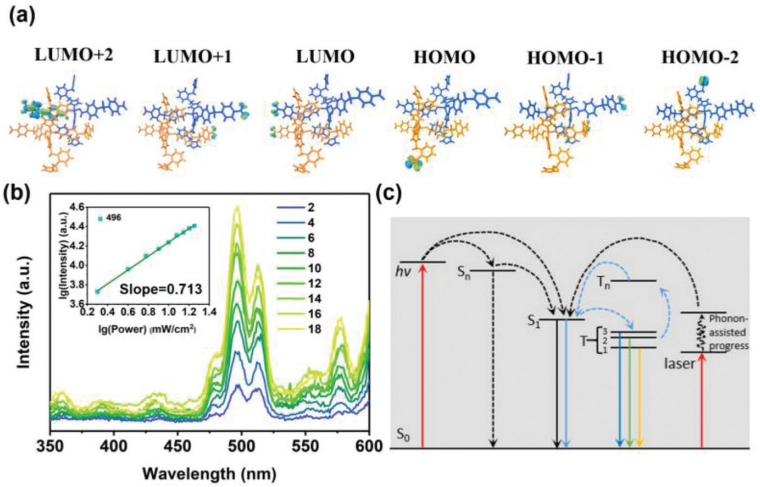

Fig. 3. (a) Calculated molecular orbitals. (b) Up-conversion emission spectra (unit: mW/cm^2, $\lambda_{ex} = 650$ nm). (c) Energy levels of different states ($h\nu$ means excitation energy) of Zn-DCPS-BIMB.

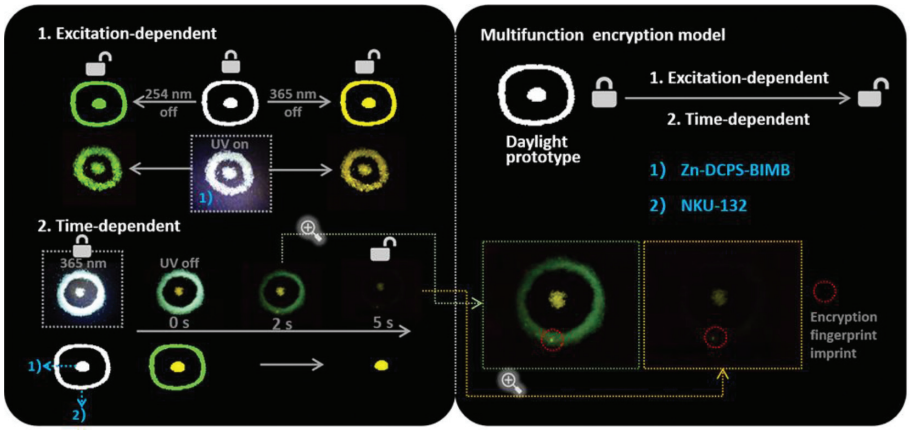

Fig. 4. The multi-functional encryption model of pattern.

the middle represents light emission. When the pattern was completely composed of Zn-DCPS-BIMB, after removing the excitation source (254 nm), we could get a green pattern, while under 365 nm excitation the pattern is yellow. The excitation-dependent afterglow color enables information to be displayed through the different colors of the pattern. When the outer circle of the pattern is composed of NKU-132 MOF [54] together with a trace amount of Zn-DCPS-BIMB crystal as the middle dot, after the 365 nm excitation light is removed, we can get time-dependent pattern display and the decoding process is shown in Fig. 4. When the excitation light source is removed for two seconds, the pattern remains the same until the green luminescence could not be detected. About 5 seconds after the excitation is stopped, we obtain a yellow dot. Besides, due to the doping of Zn-DCPS-BIMB in the outer ring NKU-132, we can find the doped yellow point in the time-dependent afterglow pattern, which serves as characteristic fingerprint encryption of the pattern.

In summary, 3D dual-ligand MOF (Zn-DCPS-BIMB) exhibits a wide-range excitation-dependent long-afterglow emission due to the introduction of multiple emission centers and orbital coupling between single and triplet states. Moreover, relying on the low-energy singlet and triplet energy levels, we provide a promising way to obtain low-energy excitation up-conversion luminescence. Taking the advantage of color-tunable ultralong RTP, the MOF has anti-counterfeiting potential for efficient information safety. It can be expected that the facile fabrication of multifunctional MOFs can be extended to other similar systems towards novel photonic applications.

Declaration of competing interest

The authors declare that they have no known competing financial interests or personal relationships that could have appeared to influence the work reported in this paper.

Acknowledgments

This work was supported by the Beijing Municipal Natural Science Foundation (No. JQ20003), the National Natural Science Foundation of China (Nos. 21771021, 21822501 and 22061130206), the Newton Advanced Fellowship award (No. NAF\R1\201285), the Fok Ying-Tong Education Foundation (No. 171008), the Measurements Fund of Beijing Normal University, and the State Key Laboratory of Heavy Oil Processing.

Supplementary materials

Supplementary material associated with this article can be found, in the online version, at doi:10.1016/j.cclet.2022.107952.

References

[1] D. Li, F. Lu, J. Wang, et al., J. Am. Chem. Soc. 140 (2018) 1916–1923.

[2] Y. Zhang, L. Gao, X. Zheng, et al., Nat. Commun. 12 (2021) 2297.
[3] L. Gu, H. Shi, L. Bian, et al., Nat. Photon. 13 (2019) 406–411.
[4] S. Kuila, S.J. George, Angew. Chem. Int. Ed. 59 (2020) 9393–9397.
[5] Y. Li, L. Jiang, W. Liu, et al., Adv. Mater. 33 (2021) 2101844.
[6] W. Zhao, T.S. Cheung, N. Jiang, et al., Nat. Commun. 10 (2019) 1595.
[7] Y. Zhang, Y. Su, H. Wu, et al., J. Am. Chem. Soc. 143 (2021) 13675–13685.
[8] L. Ma, Q. Xu, S. Sun, et al., Angew. Chem. Int. Ed. 61 (2022) e202115748.
[9] X. Li, Y. Xie, B. Song, et al., Angew. Chem. Int. Ed. 56 (2017) 2689–2693.
[10] P.R. Su, T. Wang, P.P. Zhou, et al., Natl. Sci. Rev. 9 (2022) nwab016.
[11] Q. Dang, Y. Jiang, J. Wang, et al., Adv. Mater. 32 (2020) 2006752.
[12] Q. Liao, Q. Gao, J. Wang, et al., Angew. Chem. Int. Ed. 59 (2020) 9946–9951.
[13] R. Gao, M.S. Kodaimati, D. Yan, Chem. Soc. Rev. 50 (2021) 5564–5589.
[14] X. Yang, D. Yan, Chem. Sci. 7 (2016) 4519–4526.
[15] H. Gui, Z. Huang, Z. Yuan, et al., CCS Chem. 4 (2022) 173–181.
[16] L. Ma, G. Wang, B. Ding, et al., CCS Chem. 4 (2022) 2080–2089.
[17] Q. Xu, L. Ma, X. Lin, et al., Chin. Chem. Lett. 33 (2022) 2965–2968.
[18] R. Liu, T. Jiang, D. Liu, et al., Sci. China Chem. 65 (2022) 1100–1104.
[19] C. Xu, C. Yin, W. Wu, et al., Sci. China Chem. 65 (2022) 75–81.
[20] Z. Wang, Z. Xiong, W. Liu, et al., Anal. Chem. 94 (2022) 5406–5414.
[21] R. Gao, D. Yan, D.G. Evans, X. Duan, Nano Res. 10 (2017) 3606–3617.
[22] Y. Zheng, Q. Zhou, Y. Yang, et al., Small 18 (2022) 2201223.
[23] S. Cai, H. Shi, J. Li, et al., Adv. Mater. 29 (2017) 1701244.
[24] H.J. Yu, Q. Zhou, X. Dai, et al., J. Am. Chem. Soc. 143 (2021) 13887–13894.
[25] D. Zhang, H. Zheng, X. Ma, et al., Adv. Opt. Mater. 10 (2022) 2102015.
[26] B. Wang, S. Lu, Matter 5 (2022) 110–149.
[27] M. Zhao, H. Liao, L. Ning, et al., Adv. Mater. 30 (2018) 1802489.
[28] J. Qiao, G. Zhou, Y. Zhou, et al., Nat. Commun. 10 (2019) 5267.
[29] Z. Xie, X. Zhang, H. Wang, et al., Nat. Commun. 12 (2021) 3522.
[30] H. Wang, H. Shi, W. Ye, et al., Angew. Chem. Int. Ed. 58 (2019) 18776–18782.
[31] L. Gu, H. Shi, L. Bian, et al., Nat. Photonics 13 (2019) 406–411.
[32] J. Lee, P.W. Bisso, R.L. Srinivas, et al., Nat. Mater. 13 (2014) 524–529.
[33] H. Lee, J. Kim, H. Kim, J. Kim, S. Kwon, Nat. Mater. 9 (2010) 745–749.
[34] W. Zhao, Z. He, B.Z. Tang, Nat. Rev. Mater. 5 (2020) 869–885.
[35] Y. Yang, K.Z. Wang, D. Yan, Chem. Commun. 53 (2017) 7752–7755.
[36] J. Liu, Y. Zhuang, L. Wang, et al., ACS Appl. Mater. Interfaces 10 (2018) 1802–1809.
[37] Y. Yang, X. Yang, X. Fang, K.Z. Wang, D. Yan, Adv. Sci. 5 (2018) 1801187.
[38] J. Yang, X. Gao, Z. Xie, et al., Angew. Chem. Int. Ed. 56 (2017) 15299–15303.
[39] T. Wang, Z. Hu, X. Nie, et al., Nat. Commun. 12 (2021) 1364.
[40] Z.W. Li, L.Y. Peng, X.F. Song, et al., J. Phys. Chem. Lett. 12 (2021) 5944–5950.
[41] S. Wan, J. Lin, H. Su, et al., Chem. Commun. 54 (2018) 3907–3910.
[42] Q. Peng, Z. Shuai, Aggregate 2 (2021) e91.
[43] J. Yuan, J. Dong, S. Lei, W. Hu, Mater. Chem. Front. 5 (2021) 6824–6849.
[44] C.Y. Sun, W.P. To, X.L. Wang, et al., Chem. Sci. 6 (2015) 7105–7111.
[45] Z. Wang, C.Y. Zhu, J.T. Mo, et al., Angew. Chem. Int. Ed. 133 (2020) 2556–2563.
[46] P.Y. Fu, B.N. Li, Q.S. Zhang, et al., J. Am. Chem. Soc. 144 (2022) 2726–2734.
[47] H. Liu, W. Ye, Y. Mu, et al., Adv. Mater. 34 (2022) 2107612.
[48] P. Mahato, A. Monguzzi, N. Yanai, et al., Nat. Mater. 14 (2015) 924–930.
[49] M. Scholz, G. Croizat, J. Pšenčík, et al., Photochem. Photobiol. Sci. 20 (2021) 843–857.
[50] K.T. Chan, G.S.M. Tong, W.P. To, et al., Chem. Sci. 8 (2017) 2352–2364.
[51] B. Lu, X. Fang, D. Yan, ACS Appl. Mater. Interfaces 12 (2020) 31940–31951.
[52] Y.E. Huang, X.Z. Wang, P. Hu, et al., Nanoscale 12 (2020) 6227–6232.
[53] Z. Ye, X. Lin, N. Wang, et al., Nat. Commun. 12 (2021) 4283.
[54] R. Feng, Z.Y. Li, Z.Q. Yao, et al., Sci. China Chem. 65 (2022) 128–134.